On the ρ_* Scaling of Intrinsic Rotation in C-Mod Plasmas with Edge Transport Barriers

J.E. Rice, J.W. Hughes, P.H. Diamond[♭], N. Cao, M.A. Chilenski, A.E. Hubbard, J.H. Irby, Y. Kosuga[♯]
Y. Lin, I.W. Metcalf, M.L. Reinke[†], E.A. Tolman, M.M. Victora, S.M. Wolfe and S.J. Wukitch

PSFC, MIT, Cambridge, Massachusetts 02139, USA

[♭]*UCSD, San Diego, California 92093, USA*

[♯]*Kyushu Univ, Fukuoka 816-8580, Japan*

[†]*ORNL, Oak Ridge, Tennessee 37831, USA*

Abstract

Changes in the core intrinsic toroidal rotation velocity following L- to H- and L- to I-mode transitions have been investigated in Alcator C-Mod tokamak plasmas. The magnitude of the co-current rotation increments is found to increase with the pedestal temperature gradient and q_{95}, and to decrease with toroidal magnetic field. These results are captured quantitatively by a model of fluctuation entropy balance which gives the Mach number $M_i \cong \rho_*/2\ L_s/L_T \sim \nabla T\ q_{95}/B_T$ in an ITG turbulence dominant regime. The agreement between experiment and theory gives confidence for extrapolation to future devices in similar operational regimes. Core thermal Mach numbers of $\sim$0.07 and $\sim$0.2 are expected for ITER and ARC, respectively.

1. Introduction

Substantial co-current intrinsic toroidal rotation (core Mach numbers up to 0.3) has long been observed in enhanced confinement regimes in tokamak plasmas [1, 2, 3, 4, 5, 6, 7, 8, 9]. This self-generated flow has been associated with plasma performance through a variety of global metrics such as the pressure, stored energy and confinement factor, and more recently with the edge temperature gradient, a local parameter [9]. Generally speaking, intrinsic rotation has been tied to local gradients of pressure [10] and temperature [11]. Understanding the drive mechanism of this curious phenomenon is important since in future devices without neutral beam injection, input torque will be low, so intrinsic rotation and its gradient may be necessary for suppression of MHD modes and turbulence. Originally a 'wind tunnel' approach was followed, using observations from many devices, relating engineering parameters to the measured velocity [7], but for a more reliable extrapolation to future devices, a fundamental understanding of the underlying mechanism is desirable.

It has been argued that turbulence converts thermodynamic free energy to macroscopic flow [12, 13, 14, 15]. Considering the entropy production rate balance order by order [16] gives an expression for the velocity gradient $-\chi_\phi \langle V_\parallel \rangle' + \Pi^{res} = 0$ where χ_ϕ is the momentum diffusivity and Π^{res} is the residual stress. Using a particular model of Π^{res} [16] derived considering ITG mode driven turbulence in a sheared cylinder with

$$\Pi^{res} = -\rho_* \frac{L_s}{2c_s} \chi_i \left(\frac{\nabla T}{T} \right)^2 v_{thi}^2 \tag{1}$$

where ρ_* is the normalized ion gyroradius, χ_i is the ion thermal conductivity, c_s is the ion sound speed and L_s is the magnetic shear scale length ($R_0 q/\hat{s}$), (with $v_{thi} = \sqrt{T_i/m_i}$), leads (following integration) to an expression for the Mach number [16]

$$\frac{\langle V_\parallel \rangle}{v_{thi}} \cong \frac{1}{2} \rho_* \frac{\chi_i}{\chi_\phi} \frac{L_s}{L_T} \sqrt{\frac{T_i}{T_e}} \tag{2}$$

where L_T is the temperature gradient scale length. This model will be tested in detail below.

Following a description of the experimental setup in the next section will be a presentation of the observed core velocity scaling with the pedestal temperature gradient, the edge inverse rotational transform q_{95} and the toroidal magnetic field. The observed scaling with these parameters is quantitatively compared to Eq.(2) and presented in section 4. Implications of these results are then discussed, including predicted rotation in future devices.

2. Experimental Setup

This investigation of core intrinsic toroidal rotation in enhanced confinement regimes has been undertaken on the Alcator C-Mod tokamak [17, 18], a compact (major radius

R = 0.67 m, typical minor radius of 0.21 m), high magnetic field ($B_T \leq 8$ T) device which can operate with plasma currents up to 2.0 MA. EDA H-mode [19, 18] and I-mode [20, 9, 18, 21] were accessed with up to 5 MW of ICRF heating power [22], usually at 80 MHz. At 5.4 T, this allows D(H) minority heating to be concentrated at the magnetic axis. For this scheme to work at 3.5 T, the frequency needs to be reduced to 50 MHz, but the maximum available power is then $\sim$2 MW. At low fields ($\sim$2.7 T) ICRF heating at 80 MHz can be achieved via 2^{nd} harmonic D(H). At 7.8 T, 80 MHz enables D(^{3}He) on-axis minority heating. A common feature of both H- and I-mode is the pedestal structure of the edge temperature profile [23], which is important in driving the core intrinsic rotation [9]. Electron temperature (and density) profiles were measured with Thomson scattering [24, 25]. An example of the edge electron temperature profile (and gradients) is shown in Fig.1 for a 1.3 MA, 5.4 T (q_{95}=3.4) EDA H-mode discharge with an average electron density of 5.4×10^{20}/m^3 and central electron temperature of 2.1 keV, accessed with 3.5 MW of ICRF power. Bayesian Gaussian

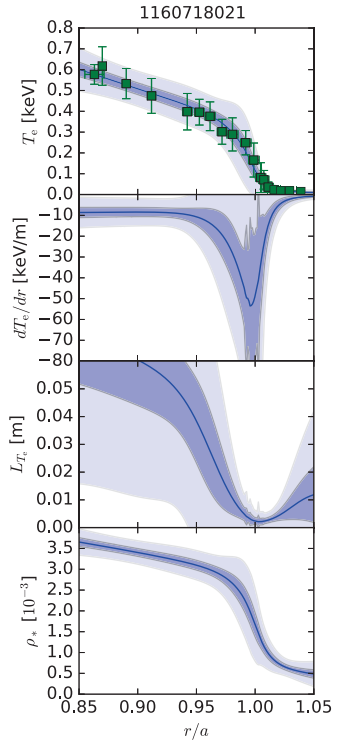

Figure 1: From top to bottom, edge profiles of the electron temperature, temperature gradient, temperature gradient scale length and normalized ion gyroradius for a 1.3 MA, 5.4 T EDA H-mode plasma. The dark shaded regions represent the $\pm1\sigma$ uncertainty envelopes for the fits and the light shaded regions are $\pm3\sigma$.

process regression [26] was used to fit the electron temperature data from the outermost 19 channels of the Thomson scattering system and the error bars represent the sample standard deviation. The nonstationary Gibbs covariance kernel with a *tanh* covariance length scale function introduced in [26] was used to capture the rapid change in temperature at the pedestal, and both the temperature and temperature gradient were constrained to go to zero at the location of the limiter. The hyperparameters which dictate the spatial structure of the profile were inferred using Markov chain Monte Carlo sampling in order to obtain a complete accounting of the uncertainty in the gradient. The uncertainties in the gradient, gradient scale length L_{T_e} and ρ_* were computed using the uncertainty propagation equation. Pedestal electron temperature gradients up to 250 keV/m have been observed, with electron temperature on the 95% flux surface reaching nearly 1 keV, and pedestal temperature gradient scale lengths from 13 mm to as small as 2.5 mm have been seen. With magnetic fields between 2.7 and 7.8 T, values of ρ_* ($\sim 10^{-4}\sqrt{\mu_i[AMU]T_i[eV]}$/B[T]a[m]) in the pedestal have been measured in the range from 1 to 4 $\times$ 10^{-3}. The working gas in all of the cases presented here was deuterium. A sample profile of ρ_* in the plasma edge is shown in the bottom frame of Fig.1. For this study, plasma currents were in the interval from 0.46 to 1.7 MA, and with B_T in the range described above leads to q_{95} between 3.0 and 6.7. Magnetic flux surfaces and q profiles were calculated using the EFIT code [27]. Representative q, magnetic shear ($\hat{s} \equiv r/q\ \partial q/\partial r$) and L_s profiles for two discharges (0.9 MA at 7.8 T and 0.7 MA at 3.5 T) are shown in Fig.2. For the 7.8 T discharge, L_s at the 95% flux

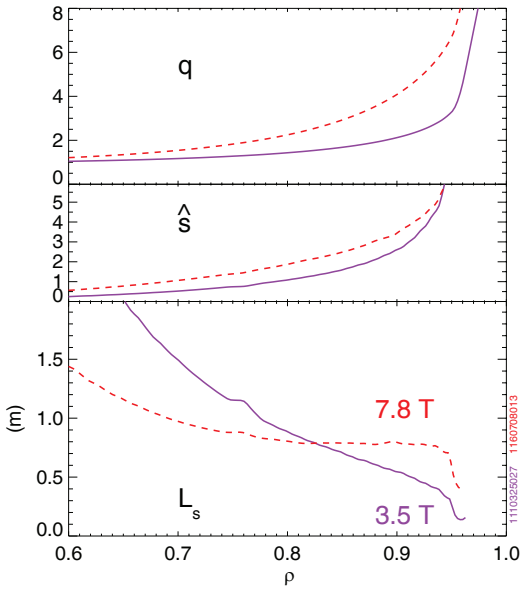

Figure 2: From top to bottom, radial profiles of the inverse rotational transform, magnetic shear and magnetic shear scale length for 7.8 (dashed line) and 3.5 T (solid line) plasmas.

surface was 0.71 m while for the 3.5 T plasma it was 0.37 m. Both of these discharges exhibited sawtooth oscillations, implying that q_0 was below unity. For the plasmas presented in this study, $L_s(0.95)$ varied between 0.37 and 0.88 m. q_{95} and L_s on the 95% flux surface are well correlated, as is demonstrated in Fig.3, which includes points from a database of $\sim$300 H- and I-mode discharges. Core ion temperature and toroidal

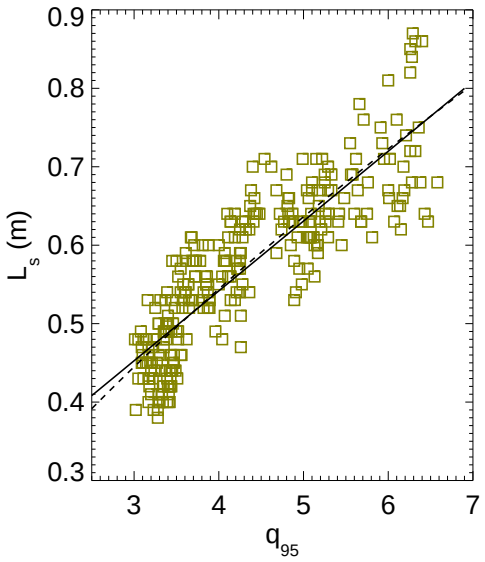

Figure 3: L_s on the 95% flux surface as a function of q_{95} for H- and I-mode discharges. Linear and power law fits are shown for comparison.

rotation profiles were measured with a high resolution imaging x-ray spectrometer system [28, 29], from observations of He- and H-like argon. Examples of chord averaged toroidal rotation velocity, ion temperature and Mach number profiles for a 1.7 MA, 7.8 T (q_{95} = 3.3) I-mode discharge are shown in Fig.4. While the velocity and temperature profiles are centrally peaked, the Mach number profile is relatively flat, at least out to r/a = 0.7. These profile shape are typical, although there may be some variation with collisionality. Velocity calibration was achieved by operating locked mode discharges (accessed with external magnetic field coils), which are presumed to have null rotation velocity [30] over the entire plasma cross section. The convention employed here defines '$+$' velocity as co-current directed rotation, while '$-$' indicates counter-current. Changes in velocity as high as 110 km/s, with central Mach numbers M_i up to 0.3 have been observed in this study. Since the core rotation velocity in the L-mode target plasmas can vary from $+20$ to -60 km/s [31, 30, 32, 8, 33, 34], all velocity scalings shown here will be of the difference between the I-/H-mode values and those of the L-mode target plasmas. A database of $\sim$300 discharges has been assembled, representing plasmas whose parameter ranges have been summarized above.

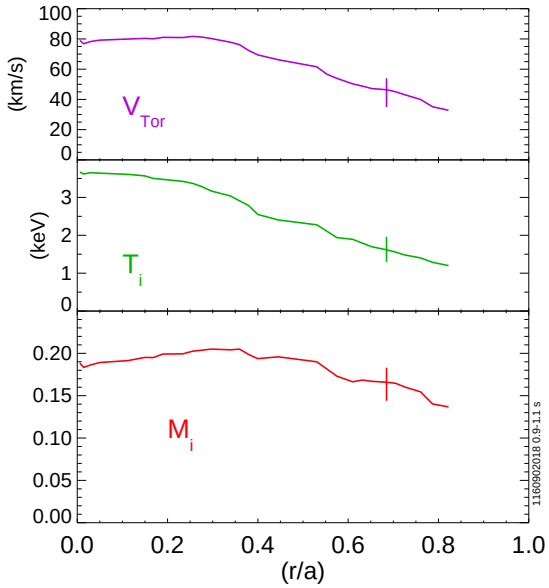

Figure 4: Radial profiles (from top to bottom) of the toroidal rotation velocity, ion temperature and Mach number for a 1.7 MA, 7.8 T I-mode plasma.

3. Observed Toroidal Rotation Scalings

Shown in Fig.5 are the time histories of parameters of interest for a 7.8 T, 0.9 MA (q_{95} = 6.3) EDA H-mode plasma accessed with 3 MW of ICRF power at 80 MHz. Following the H-mode transition at 0.62 s, there were the usual increases observed in the plasma stored energy, electron density and temperature, pedestal temperature gradient and core toroidal rotation velocity. In this case the pedestal electron temperature gradient increased to about 120 keV/m followed by a change in the toroidal rotation (co-current) by $\sim$60 km/s, consistent with earlier results [9]. Notice that after the ICRF fault ($\sim$1.15 s), there was a brief drop in the pedestal temperature gradient and loss of H-mode followed by a decrease in the core velocity and density, before recovery. The relationship between the core toroidal velocity and the pedestal temperature gradient is explored in Fig.6 for 5.4 T H- and I-mode plasmas. There is a strong correlation between the two, captured by the scaling $V \propto (\nabla T)^{0.8}$ (solid curve). Data points from H- and I-mode plasmas are interspersed, indicating very similar rotation characteristics [9]. There is no evidence for a critical gradient necessary to drive the rotation. Some of the scatter is due to the inverse dependence of the velocity on plasma current [3, 7]; the range of currents in Fig.6 is from 0.55 to 1.3 MA, with q_{95} between 6.7 and 3.0. Looking ahead to a comparison of rotation in plasmas with different toroidal magnetic fields, it is prudent to utilize q_{95} as the variable rather than I_p. This dependence on q_{95} is presented in Fig.7 which shows the velocity increase with q_{95} at fixed pedestal

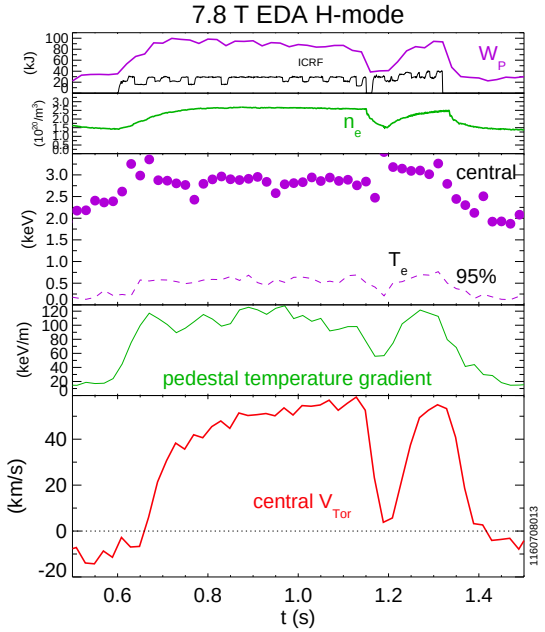

Figure 5: Time histories, from top to bottom, of the plasma stored energy (and ICRF power waveform), average electron density, central (dots) and pedestal (dashed line) electron temperature, pedestal temperature gradient and core toroidal rotation velocity for a 7.8 T EDA H-mode discharge.

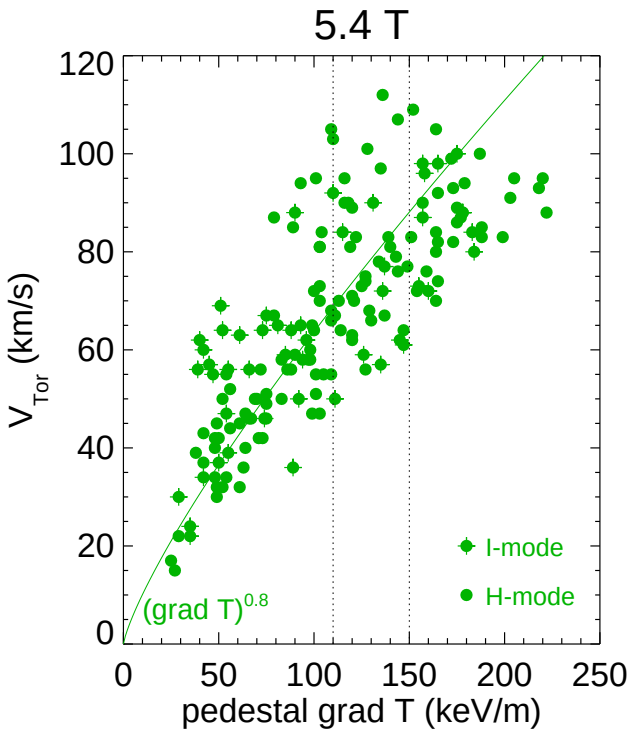

Figure 6: The change in the central toroidal rotation velocity as a function of the pedestal electron temperature gradient for 5.4 T H- and I-mode plasmas. The curve is proportional to $(\nabla T)^{0.8}$.

temperature gradient for 5.4 T discharges, from the region between dotted vertical lines in Fig.6 (with ∇T between 110 and 150 keV/m). The nearly linear increase with q_{95} is

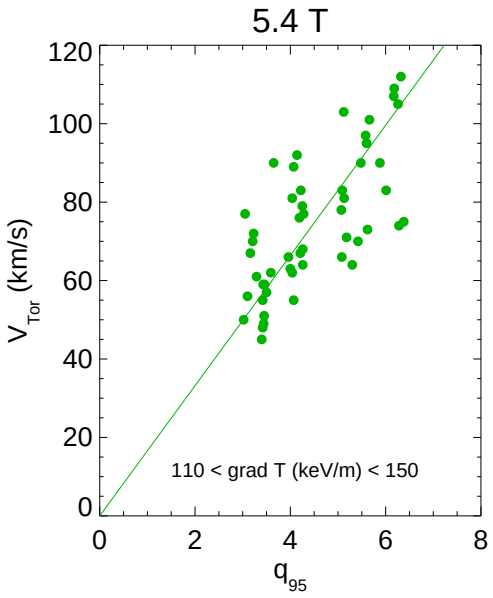

Figure 7: The change in the central toroidal rotation velocity as a function of q_{95} for 5.4 T I- and H-mode plasmas with pedestal temperature gradients between 110 and 150 keV/m.

apparent.

The dependence of intrinsic rotation on toroidal magnetic field has been investigated in plasmas with a range of B_T from 2.7 to 7.8 T. There are two approaches to this. The first is to examine the change in velocity with magnetic field for fixed values of both q_{95} and the edge temperature gradient, independently. Examples are shown in Fig. 8 for two cases: plasmas with edge temperature gradients between 45 and 65 keV/m with $3 < q_{95} < 4$ (squares) and those cases with edge temperature gradients between 100 and 140 keV/m and q_{95} from 4 to 5 (diamonds). There is a clear decrease in the velocity as a function of magnetic field for fixed q_{95} and edge temperature gradient. A drawback of this approach is that the range of magnetic field for fixed q_{95} and ∇T is limited. The second approach is to consider a fixed value of the $q_{95}\times\nabla$T product. The change in the central rotation velocity as a function of the product of q_{95} and the pedestal electron temperature gradient, suggested by the results from Figs.6 and 7, is shown in Fig.9 for I- and H-mode plasmas with toroidal magnetic field in three ranges: 2.7 - 3.5 T (triangles), 4.8 - 6.1 T (dots) and 7.8 T (asterisks). There is a marked increase of the observed velocity with the product $q_{95}\times\nabla$T. The points appear to be ordered by magnetic field, with a larger velocity response to a given increase in the $q_{95}\times\nabla$T product apparent for lower B_T. Although the range in ∇T achieved for low

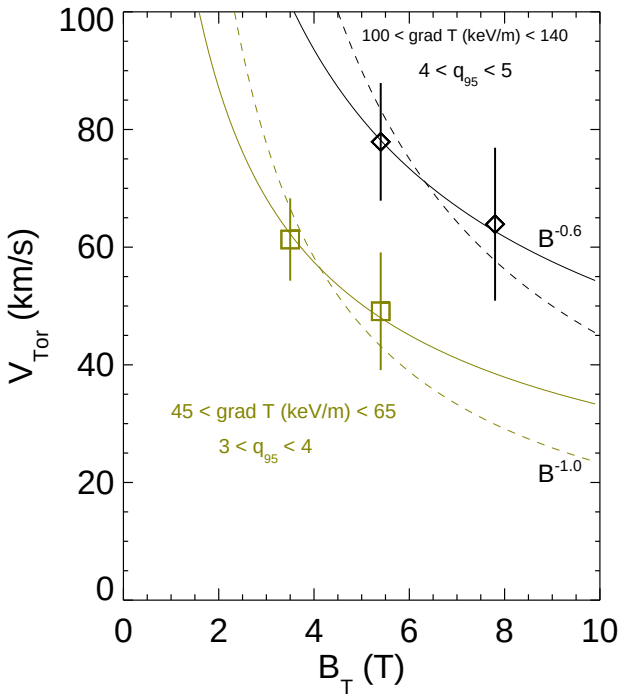

Figure 8: The change in the central toroidal rotation velocity as a function of toroidal magnetic field for plasmas plasmas with edge temperature gradients between 45 and 65 keV/m with $3 < q_{95} < 4$ (squares) and those cases with edge temperature gradients between 100 and 140 keV/m with q_{95} from 4 to 5 (diamonds). Curves proportional to $B^{-0.6}$ (solid) and 1/B (dashed) are shown for comparison.

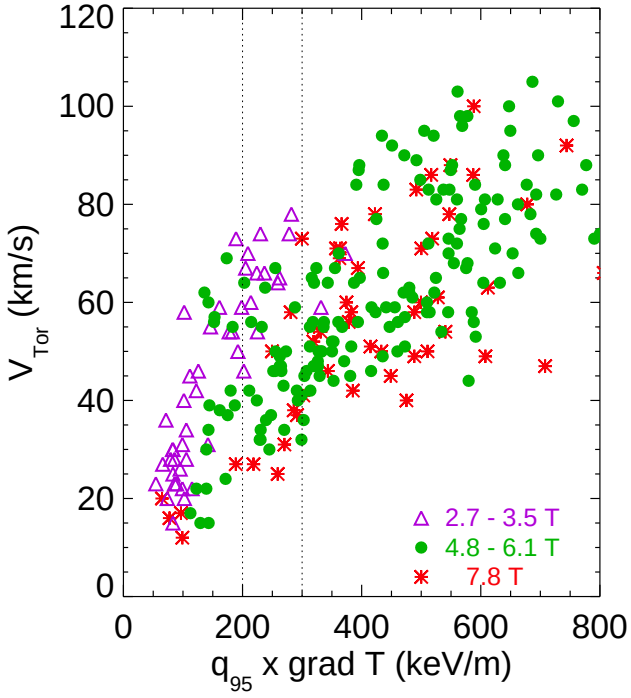

Figure 9: The change in the central toroidal rotation velocity as a function of the product $q_{95} \times \nabla T$, sorted by toroidal magnetic field: 2.7 - 3.5 T (triangles), 4.8 - 6.1 T (dots) and 7.8 T (asterisks).

field plasmas was limited by available ICRF power at 50 MHz, it is possible to compare plasmas for three magnetic fields for a subset of data with $q_{95}\times\nabla T$ between 200 and 300 keV/m, as depicted by the pair of vertical lines in Fig.9. The change in the central toroidal velocity as a function of B_T is shown in Fig.10 for plasmas with $q_{95}\times\nabla T$ in this range. There is a marked decrease with increasing magnetic field. Shown for com-

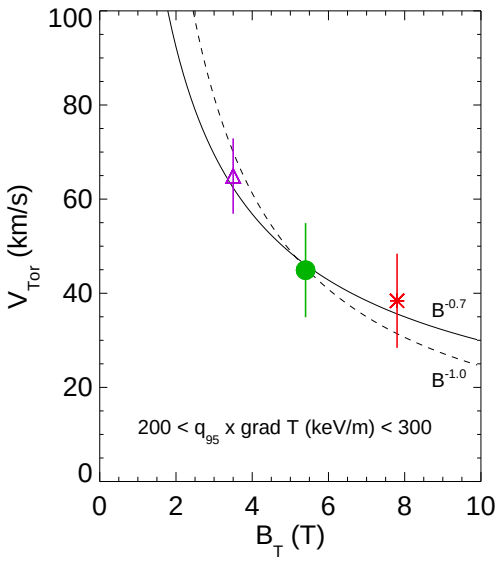

Figure 10: The change in the central toroidal rotation velocity as a function of toroidal magnetic field, with the product of q_{95} and the pedestal electron temperature gradient between 200 and 300 keV/m. Curves are proportional to $B^{-0.7}$ (solid) and 1/B (dashed).

parison are curves scaling as $B^{-0.7}$ (solid) and 1/B (dashed). This scaling is consistent with that from Fig.8.

To summarize the results of this section, the change in the central toroidal rotation velocity, ΔV, increases with the pedestal electron temperature gradient and q_{95}, and decreases with toroidal magnetic field as $\Delta V \sim \nabla T^{0.8\pm0.3}\ {q_{95}}^{1.0\pm0.2}\ / B^{0.7\pm0.4}$.

4. Comparison with Model

These results may be compared to the model of Eq.(2), noting that it simplifies to

$$M_i \cong \frac{1}{2}\rho_* \frac{L_s}{L_T} \tag{3}$$

assuming a Prandtl number (χ_i/χ_ϕ) of unity and $T_e = T_i$. It is very difficult to measure χ_ϕ in plasmas with only intrinsic rotation since the source is not well characterized, and modulation experiments are difficult. Some information can be gleaned from the rise of the velocity following the L-H or L-I transition, as seen in the bottom frame of Fig.5. The origin of core velocity is in the pedestal [35, 30, 9]; fitting an hyperbolic tangent function to the core velocity rise yields a single parameter which can be interpreted as the global momentum confinement time. This velocity rise time has been determined for a large number of H- and I-mode discharges, and is shown in Fig.11 as a function of the global energy confinement time. There is a good correlation between

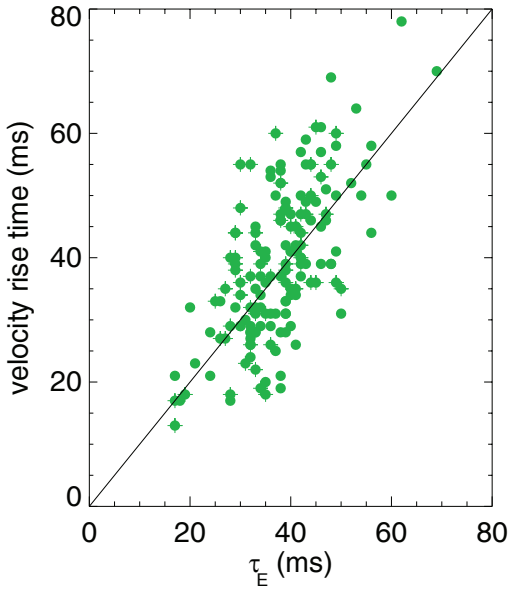

Figure 11: The velocity rise time following the L-H (dots) and L-I (dots with plus signs) transition as a function of the global energy confinement time for 5.4 T discharges.

the two, and the values are similar, suggesting that energy and momentum confinement are tied together. In the following, the Prandtl number χ_i/χ_ϕ is taken to be 1, which is commonly observed in neutral beam heated plasmas and is also consistent with theoretical fundamentals. Furthermore, the ion temperature is not routinely measured in the pedestal, but from comparisons when available, it is always found that $T_i = T_e$ near the plasma edge. This serves as justification of the two assumptions mentioned above. Eq.(3) reduces to $M_i \propto \nabla T\ q_{95}/B$ if $q \sim r\nabla q$, and nicely reproduces the observed scalings from the previous section.

An issue of importance regards where in the plasma cross section Eq.(3) should be evaluated. Since the source of the co-current intrinsic rotation in H- and I-mode plasmas is at the edge [35, 30, 9], and the temperature pedestal forms as a result of the confinement regime transition, it is natural to choose the maximum temperature

gradient in the pedestal, with ρ_* and L_s taken at the pedestal top. Rotation in the pedestal is also not routinely measured; the large body of rotation data is from the core x-ray system. Since the Mach number profile is relatively flat (Fig.4), in the following the central Mach number will be used. With these *caveats*, it is possible to test the model of Eq.(3) against the experimental observations of section 3. Unfortunately it isn't possible to vary ρ_*, L_s or L_T independently, holding the other two constant. For example changing the edge temperature gradient changes the temperature at the pedestal top, which changes ρ_*. Varying the magnetic field to change ρ_* also changes L_s.

Shown in Fig.12 is the experimental Mach number as a function of $1/2\rho_* L_s/L_T$ for a large number of H- and I-mode discharges. Values for different magnetic fields are

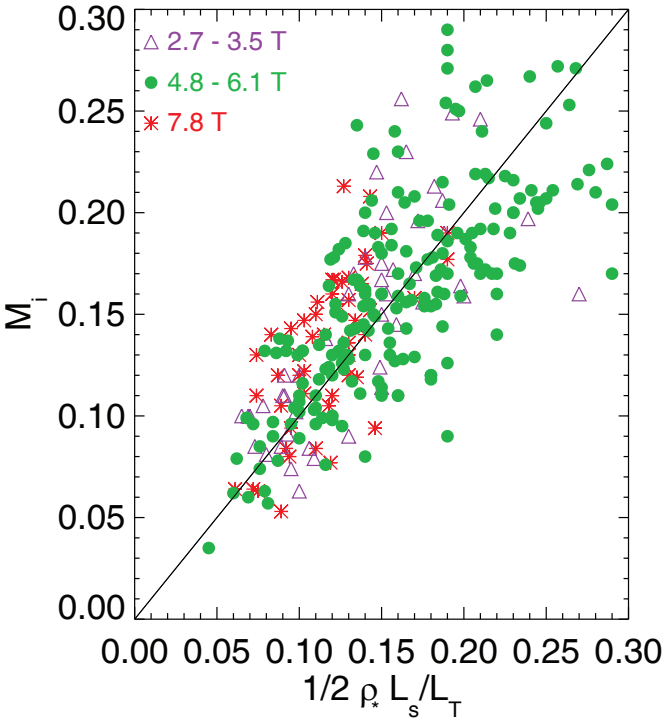

Figure 12: The experimental Mach number as a function of $1/2\rho_* L_s/L_T$ for H- and I-mode discharges, sorted by magnetic field.

interspersed. The agreement with the model is outstanding, over nearly an order of magnitude. This agreement justifies the order by order entropy production rate balance paradigm, as well as the analytic model of the residual stress in the ITG turbulence dominated regime given by Eq.(1). The dependence on ρ_* shown in Fig.12 is opposite to the ${\rho_*}^{-1.5}$ scaling found in DIII-D plasmas [36].

5. Discussion and Conclusions

The agreement between observations and theory shown in Fig.12 supports the ITG mode dominant model driven by the edge temperature gradient (∇T) in a sheared magnetic field (L_s) scaling with the normalized ion gyroradius (ρ_*). The basic ρ_* scaling emerges from the relation $\langle V_\parallel \rangle' \sim \Pi^{res}/\chi_\phi$, where Π^{res} is a non-diffusive stress. In terms of scalings, $\Pi^{res} \sim (V_{dia})^2 \sim {\rho_*}^2 {c_s}^2$, while $\chi_\phi \sim V_{dia}\rho \sim \rho_* c_s \rho \sim D_{GB}$. Note that the $\hat{s} \sim 2$ environment of the pedestal motivates the case of the sheared cylinder ITG model. Some caution should be exercised here as additional ρ_* dependence may enter *via* the symmetry breaking factor, which is sensitive to several complex details and may change with plasma parameters and radial location.

The expression for the Mach number Eq.(3) works very well for C-Mod observations, capturing the scalings with edge temperature gradient, q_{95} and B_T, and it may be applied to future devices in order to get an estimate of the expected intrinsic rotation. For ITER Q=5 and Q=10 H-mode scenarios [37], with pedestal ρ_* values of $\sim$0.001, L_T $\sim$0.06 m and L_s $\sim$8 m, the predicted Mach number is $\sim$0.07, which corresponds to a core toroidal rotation velocity of $\sim$50-75 km/s, depending on the core temperature and velocity peaking, and is large enough to suppress RWMs. This estimate is considerably lower those from a multi-machine scaling comparison [7], which didn't account for the edge temperature gradient drive. Interestingly, these predictions are very close to those with an opposite ρ_* scaling [36]. For ARC [38] (a = 1.1 m, B = 9.2 T), with predicted pedestal ρ_* = 0.0016, L_T = 0.025 m and L_s = 6 m, the Mach number estimate is 0.2, which yields a substantial core velocity of over 200 km/s for a central temperature of 27 keV.

6. Acknowledgements

The authors appreciate enlightening discussions with A. Loarte, A. Polevoi and D. Whyte, and thank the Alcator C-Mod operations and ICRF groups for expert running of the tokamak. Work supported at MIT by DoE Contract No. DE-FC02-99ER54512 and at UCSD by DoE Contract No. DE-FC02-04ER54738.

References

[1] L.-G.Eriksson *et al.*, 1997 *Plasma Phys. Contr. Fusion* **39** 27.

[2] J.E.Rice *et al.*, 1998 *Nucl. Fusion* **38** 75.

[3] J.E.Rice *et al.*, 1999 *Nucl. Fusion* **39** 1175.

[4] G.T.Hoang *et al.*, 2000 *Nucl. Fusion* **40** 913.

[5] L.-G.Eriksson *et al.*, 2001 *Nucl. Fusion* **41** 91.

[6] J.E.Rice *et al.*, 2001 *Nucl. Fusion* **41** 277.

[7] J.E.Rice *et al.*, 2007 *Nucl. Fusion* **47** 1618.

[8] J.E.Rice *et al.*, 2008 *Plasma Phys. Contr. Fusion* **50** 124042.

[9] J.E.Rice *et al.*, 2011 *Phys. Rev. Lett.* **106** 215001.

[10] M.Yoshida *et al.*, 2008 *Phys. Rev. Lett.* **100** 105002.

[11] K.Ida *et al.*, 2010 *Nucl. Fusion* **50** 064007.

[12] Ö.D.Gürcan *et al.*, 2007 *Phys. Plasmas* **14** 042306.

[13] P.H.Diamond *et al.*, 2008 *Phys. Plasmas* **15** 012303.

[14] P.H.Diamond *et al.*, 2009 *Nucl. Fusion* **49** 045002.

[15] Ö.D.Gürcan *et al.*, 2010 *Phys. Plasmas* **17** 112309.

[16] Y.Kosuga *et al.*, 2010 *Phys. Plasmas* **17** 102313.

[17] E.S.Marmar *et al.*, 2007 *Fusion Sci. Technol.* **51** 261.

[18] M.Greenwald *et al.*, 2014 *Phys. Plasmas* **21** 110501.

[19] M.Greenwald *et al.*, 1997 *Nucl. Fusion* **37** 793.

[20] D.G.Whyte *et al.*, 2010 *Nucl. Fusion* **50** 105005.

[21] A.E.Hubbard *et al.*, 2016 *Nucl. Fusion* **56** 086003.

[22] P.T.Bonoli *et al.*, 2007 *Fusion Sci. Technol.* **51** 401.

[23] J.W.Hughes *et al.*, 2013 *Nucl. Fusion* **53** 043016.

[24] J.W.Hughes *et al.*, 2001 *Rev. Sci. Instrum.* **72** 1107.

[25] N.P.Basse *et al.*, 2007 *Fusion Sci. Technol.* **51** 476.

[26] M.A.Chilenski *et al.*, 2015 *Nucl. Fusion* **55** 023012.

[27] L.L.Lao *et al.*, 1985 *Nucl. Fusion* **25** 1611.

[28] A.Ince-Cushman *et al.*, 2008 *Rev. Sci. Instrum.* **79** 10E302.

[29] M.L.Reinke *et al.*, 2012 *Rev. Sci. Instrum.* **83** 113504.

[30] J.E.Rice *et al.*, 2004 *Nucl. Fusion* **44** 379.

[31] J.E.Rice *et al.*, 1997 *Nucl. Fusion* **37** 421.

[32] J.E.Rice *et al.*, 2005 *Nucl. Fusion* **45** 251.

[33] J.E.Rice *et al.*, 2011 *Nucl. Fusion* **51** 083005.

[34] J.E.Rice *et al.*, 2013 *Nucl. Fusion* **53** 033004.

[35] W.D.Lee *et al.*, 2003 *Phys. Rev. Lett.* **91** 205003.

[36] C.Chrystal *et al.*, 2016 *Phys. Plasmas* submitted, “Scaling of Intrinsic Torque and Momentum Confinement with Normalized Gyroradius and Collisionality in the DIII-D Tokamak”

[37] A.R.Polevoi *et al.*, 2017 *Nucl. Fusion* **57** 022014.

[38] B.N.Sorbom *et al.*, 2014 *Fusion Eng. Des.* **100** 378.